Cellular Automa: prospects in astrophysical applications, eds: J.M. Perdang, A. Lejeune, World Scientific, 1993

THE SIMULATION OF UNIVERSAL MULTIFRACTALS

S. PECKNOLD, S. LOVEJOY, D. SCHERTZER*
C. HOOGE, J.F. MALOUIN
Department of Physics, McGill University
3600 University St., Montréal, Québéc, H3A 2T8, Canada

ABSTRACT

The existence of multifractal fields in nature is recognized as a widespread phenomenon, one which describes a multitude of different systems. It is therefore necessary to develop an understanding of their behaviour. Simulations play an important role in this understanding. They are used to evaluate new analysis techniques, to determine if results are reproducible according to a theoretically correct model, and particularly to simulate complex interactions in geophysical fields, such as radiative scattering in clouds and the forecasting of weather and earthquakes. They are also necessary for developing sampling, averaging and calibration procedures for remotely sensed geophysical and astrophysical fields. Thus, it is necessary to have a method of producing simulations of all the possible cases of interest. These simulations may be produced for fields and time series with many different parameters, including the sparseness of the actual field, differing probability distributions and spectra, as well as those that exhibit anisotropic scale invariance, e.g. stratified or differentially rotated fields.

1. Introduction

A growing body of geophysical research is devoted to determining the scaling properties of fields that arise in nature as a result of nonlinear processes acting over wide ranges in scale. Geophysical fields including rainfall and cloud fields[1,2], temperature fields[3], topography[4] and the roughness of the ocean surface[5] and wind tunnel turbulence[6] have been analyzed over various time and space scales and have been shown to be multifractal in nature. In addition, such phenomena as earthquakes[7] and sea ice[8], as well as

* *L. M. D./C.N.R.S., BP 99, Université Pierre et Marie Curie*
4 Place Jussieu F-75252 Paris Cedex 05, France

apparent galactic luminosity[9] have been analyzed and shown to have fractal distribution, and further research has demonstrated that all these fields are in fact multifractal in nature.[10,11,12,13] As well, analysis of human speech[14], high energy hadron jets[15] and pollution distribution from the Seveso industrial accident[16] have all demonstrated that multifractal fields arise in many disparate situations. (Universal multifractal parameters are discussed in Section 2 and a fairly complete list of known results is summarized for these fields in Table 1.)

Given this ubiquity of multifractal fields, techniques to model them must be developed. The early scaling models of geophysical fields were based on an assumption of "simple scaling"[17,18], resulting in the description of the field by a single fractal dimension. The physical processes were thus modeled as monofractals, simulations of which were produced by summing many random structures (e.g. the FSP model[18]), by simply filtering white noise (this is how Voss[19] created his impressive monofractal mountainscapes), or by variations on these processes such as "midpoint displacement"[20] or more recently "iterated function systems"[21].

None of these models provide an adequate description of the actual physical nonlinear dynamic process involved. The first step in this direction was the use of multiplicative (nonlinear) processes which emerged from the study of turbulent cascade processes. At first, great attention was paid to the monofractal special case, the "β-model"[22,23,24,25], but this was shown to be unstable to small perturbations (which yielded the multifractal "α-model"[26]. From the point of view of physical modeling, these early multifractal models had several defects: they had discrete rather than continuous spectra (which in addition, gave rise to ugly straight-line structures), but more fundamentally, they involved an infinite number of parameters for their specification (the dimension function). This made it highly unlikely that sufficient theoretical or empirical information would ever be available to enable realistic models to be produced.

It turned out that the solutions to both problems were closely linked. The discrete cascade actually simultaneously involved two limiting processes; the small scale limit and the limit of an infinite number of interactions. By separating the two limits and considering the densification (or more generally nonlinear "mixing" of processes) over a finite range of scales, it was shown[27,28] that due to the existence of stable, attractive "universal" generators of multifractal processes, that many of their dynamical details could be washed out *if sufficiently many nonlinear interactions were available over a finite range of scales.* For universal multifractals, only three basic parameters are necessary to specify the entire process (including the infinite hierarchy of fractal dimensions).

However, important as it was to replace the linear monofractal models by nonlinear multifractal models, such models involved self-similar multifractals in which the small and large scale statistical properties were related by a simple "zoom" or magnification. On the contrary, geophysical fields are seldom (if ever) isotropic, and the operator required to go from large to small scale typically involves reduction coupled with compression, rotation or more complex operations which can vary not only with scale, but also with location. Such anisotropy is associated for example with texture and morphology. The formalism necessary to define the notion of scale and scale change in such an anisotropic framework is Generalized Scale Invariance (GSI)[29,30]. The final step in making physically realistic multifractal models is to therefore to combine continuous cascades (sections 2, 3) with GSI operators (see section 5).

In this paper we bring up to date the techniques of simulating universal multifractals and show for the first time how to combine the use of GSI with the continuous multiplicative simulation technique to provide the most realistic possible model of nonlinear dynamical scale invariant processes. In addition, former problems such as the previous inability to simulate universal multifractals over certain ranges of the parameters have been resolved. It is now possible to simulate universal multifractals over the entire theoretically possible range. Finally, an attempt is made to provide a visual catalogue demonstrating the effects of altering the parameters describing multifractality.

2. Universal Multifractals

From fractals to Multifractals

The transition from a fractal set to a multifractal field is fundamental in terms of the resulting mathematical structure yet is not conceptually difficult to understand. The distinction is that in a (mono-)fractal set we obtain a single value for the dimension, whereas with a multifractal field we can define a series of sets (e.g. using thresholds) each of which will have its own (generally different) dimension. Given a multifractal field, we can look at the sub-sets corresponding to thresholding at each given value. For example, in Fig.1, we look at this type of field, analyzed at scale ratio λ (for example, the ratio between image size and pixel size in an image). The thresholds chosen are λ^{γ_1} and λ^{γ_2}. The points corresponding to field values ε_λ greater than these thresholds form geometric subsets, as long as the corresponding dimension is positive. With each of these geometric sub-sets we can find an associated fractal dimension. If we look at the probability of finding a field value greater than a given (scale dependent) threshold, we find[28] that the probability, $\Pr(\varepsilon_\lambda > \lambda^\gamma)$, can be related to the order of singularity, γ, by :

$$\Pr(\varepsilon_\lambda > \lambda^\gamma) \approx \lambda^{-c(\gamma)} \qquad (1).$$

where ε_λ corresponds to a singularity of order γ and the codimension function, $c(\gamma)$, describes the *sparseness* of the field intensities: when smaller than the dimension of the space in which the process is observed, the codimension is the difference between the dimension of space and the fractal dimension of the geometric subset described by the singularity value. It should be noted that when the codimension is larger than the dimension of support (i.e. the dimension of the embedding space), the meaning is that in any given realization, the corresponding values ε_λ are almost surely not found: $c(\gamma)$ is related to the probability density, and field values with arbitrarily large codimension can appear because the probability space defining the process is infinite-dimensional[31].

Although the codimension function $c(\gamma)$ yields the entire statistical description of the multifractal field, it can only be determined by empirical methods; there is no theoretical form for the function, beyond that determined by the fact that it gives a probability density (which only implies convexity). A more powerful result is what are called *universal multifractals*[31], for which we will be able to write an explicit functional form for the codimension function.

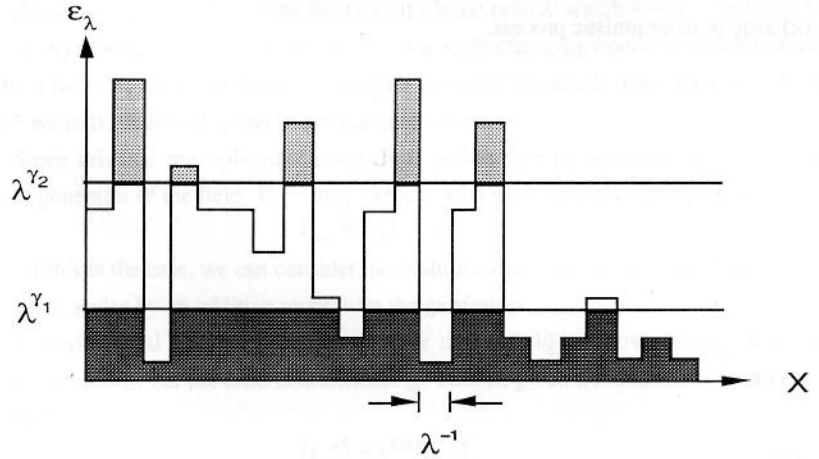

figure 1—A schematic illustration of a multifractal field analyzed over a scale ratio λ, with two scaling thresholds $\lambda^{\gamma_1}$and. λ^{γ_2}, corresponding to two orders of singularity : $\gamma_2>\gamma_1$. (Lovejoy and Schertzer(32))

Multifractals can arise in nonlinear systems with both small and large numbers of degrees of freedom. In the former, a few degrees of freedom characterize the probability measure or phase space of the system; these systems are associated with calm, geometric multifractals[33]. On the other hand, turbulent and turbulent-like systems involving many degrees of freedom (e.g. fields) are often associated with stochastic cascade processes and generally lead to wild and hard multifractals[33]. Geophysical and astrophysical applications typically involve fields; we illustrate the cascade process using the example of the turbulent energy flux ε_λ. The energy flux is injected into the system at a large scale cascades down to smaller scales by successive multiplicative modulation down to a very small scale dissipative regime. Figure 2 shows a schematic treatment of the cascade process. In this figure, showing a discrete cascade, independent random increments $\mu\varepsilon$ are generated at each scale, proceeding in factors of two, and the field is multiplicatively modulated with them: the energy is redistributed by boosts and decreases as one moves to smaller and smaller scales. It is termed *isotropic* because the boxes are of the same shape (in this case they are square).

When the redistribution of the cascading quantity ε is uneven between the boxes, it gives rise to what is called intermittency[34,35]. This unevenness could be caused by either a stochastic or deterministic process.

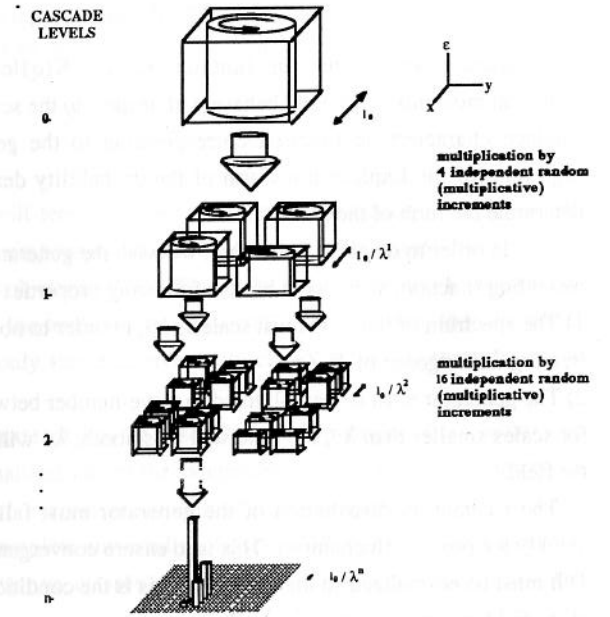

Figure 2—A schematic diagram showing a few steps of a discrete multiplicative cascade process.(30)

Properties of Multifractals

In order to simulate the field of interest, ε, we look at its behaviour at different scales. Using ε_λ as the field at a scale ratio λ, we look at the field at a scale ratio $\lambda\lambda'$. Comparing this to the field at a scale ratio λ, we note that for a multiplicative cascade process the field $\varepsilon_{\lambda\lambda'}$ should be statistically the same as taking the field at a scale ratio λ and multiplying each "box" of size $1/\lambda$ by the field at a scale ratio λ' which has been reduced by a factor λ. Symbolically, $\varepsilon_{\lambda\lambda'} = T_\lambda(\varepsilon_{\lambda'})\varepsilon_\lambda$. T_λ is a scale changing operator which reduces scales by a factor λ; for the moment we consider isotropic (standard) reductions in scale. In section 5 we indicate how this can be greatly generalized.

Since this is a multiplicative property it is therefore convenient to introduce an (additive) generator of the field, $\Gamma_\lambda = \ln \varepsilon_\lambda$, which satisfies the additive group property[32]:

$$\Gamma_{\lambda\lambda'} = T_\lambda \Gamma_{\lambda'} + \Gamma_\lambda \qquad (2)$$

Given that this is the case, we can consider the multiplicative field as being produced down to very small scales by an additive process on the generators.

In multifractal fields, different moments of the field are governed by different power-law relations: i.e. the field is multiscaling. That is, given a multifractal field ε_λ at a scale ratio[28] λ,

$$\langle \varepsilon_\lambda{}^q \rangle = \lambda^{K(q)} \langle \varepsilon_1{}^q \rangle \qquad (3)$$

Hence, we have a function K(q) depending on the moment of our field that describes how the statistical properties of each moment behave under isotropic dilations and contractions.

Considering for convenience a normalized field at the largest scale, i.e. $\langle \varepsilon_1^q \rangle = 1$, we can rewrite Eqn.(3) in terms of the generator[28,31] :

$$\left\langle \varepsilon_\lambda^q \right\rangle = \left\langle \exp(q\Gamma_\lambda) \right\rangle = \exp(K_\lambda(q)) = \lambda^{K(q)} \tag{4}$$

This equation shows that the function $K_\lambda(q) = K(q)\log(\lambda)$ that describes how the statistical moments of the field behave with respect to the scale ratio λ is actually the second Laplace characteristic function corresponding to the generator[31,37] Γ_λ, that is, the logarithm of the Laplace transform of the probability density. Given this, we can now determine the form of the generator.

In order to obtain multiscaling, we wish the generator to be a noise with a possible weighting function, such that it has the following properties[32]:

1) The spectrum of the field must scale as k^{-1}, in order to obtain the scaling behaviour: that is, a $\log\lambda$ divergence of $K_\lambda(q)$.

2) The generator must be band-limited to wave-number between $[1,\lambda]$; this is to ensure that for scales smaller than λ^{-1}, the field will be smooth; λ^{-1} will therefore be the resolution of the field.

3) The probability distribution of the generator must fall off more than exponentially quickly for positive fluctuations. This is to ensure convergence of K(q) for q>0.

4) It must be normalized so that K(1)=0. This is the condition of conservation of the mean of the field at varying scales; $\langle \varepsilon_\lambda \rangle = 1$.

Having noted these properties, it now remains to determine the type of noise generator to use. As mentioned in the introduction, we know little about the functional form of the codimension function, and thus the K(q) function, beyond the very general restrictions placed upon them until now. The abandonment of the geometric monofractal approach to nonlinear variability for the less restrictive and more accurate multifractal approach was necessary for the proper understanding of actual physical processes. However, in effect, we have traded the description of our nonlinear process via a single parameter (the fractal dimension), for an infinity of parameters describing the hierarchies of dimensions and singularities. This situation is rectified by the introduction of universal multifractals, whereby we can once again describe nonlinear variability in terms of a few fundamental parameters, where these parameters are no longer geometric, but dynamic[31]. We can observe how these parameters, and thus the universality classes they describe, arise by considering the generator of a multiplicative cascade. We therefore examine the properties of the sums of random noises, corresponding to the additive process on the generator of the field, by looking at the problem of random walks[36], which are additive processes.

A random walk in d dimensions is merely the addition of independent random vectors $\mathbf{x}_1, \mathbf{x}_2, \ldots$, with random direction and random length. Let us assume (for now) finite variance of the length. Here we take the expectation or mean of the length = 1. Then the normalized sum of this random walk has its distribution tend toward the normal distribution[36]:

$$\mathbf{S}_n = \frac{\mathbf{X}_1 + \mathbf{X}_2 + \ldots + \mathbf{X}_n}{\sqrt{n}}$$
$$c_{ij} = \delta_{ij}/d \tag{5}$$

where the distribution of $\mathbf{S}_n$ will tend towards the normal distribution as $n \to \infty$. The covariance matrix of the d components of each vector, c_{ij} (the usual for a normal distribution) will be diagonal with elements 1/d. This is the standard central limit theorem. Although for historical reasons the terminology "universal" is seldom used in this context, this is in fact the most commonly studied universality class for the addition of random variables.

This procedure can be extended to the case where the variances of the vectors are not finite. In this case, the normalized sum of the independent vectors has a distribution that tends toward any member of a class of probability distributions, known as Lévy distributions, which form the complete universality classes of addition of random variables (they are the only stable, attractive classes of random variables under addition). The analogue of Eqn.(5) is[36]

$$\mathbf{S}_n = \frac{\mathbf{X}_1 + \mathbf{X}_2 + \ldots + \mathbf{X}_n}{n^{1/\alpha}} \tag{6}$$

where $\mathbf{S}_n$ has the property that the distribution $\mathbf{S}_n + b_n$ tends toward the distribution of the random variables $\mathbf{x}_i$, characterized by the Lévy parameter α, taking on values $0 < \alpha \leq 2$. The term b_n is a recentering term, required for $\alpha > 1$, such that the distribution is centered to zero expectation.

Although the probability density of most members of this class cannot be written in closed form, the characteristic function can be. In fact, the second Laplace characteristic function of this type of random variable, assuming convergence, has the form[37]:

$$K(q) \propto q^\alpha, \quad 0 < \alpha \leq 2, \ \alpha \neq 1$$
$$K(q) \propto q\ln(q), \qquad \alpha = 1 \tag{7}$$

where α is the Lévy parameter describing the probability distribution of the noise (in fact α is the exponent of the power-law fall-off of the tail of the probability density[36]).

In our case, we wish to obtain the continuous limit of a multiplicative cascade[31,38]. As a discrete cascade proceeds to the small scale limit, we are in fact taking two limits; an infinite number of random variables and the limit of infinitely small scales. In this case the normalization condition (condition 4) implies that $\langle \Gamma_\lambda \rangle < 0$ which is not in general compatible with the centering and normalization required for the central limit theorem to

apply. The result is that discrete cascades will generally not tend to universal limits (a fact that has unfortunately obscured the issue of universality and even lead to claims that no universality classes exist[39]). However, if on the contrary we first keep the total scale ratio λ fixed and finite and proceed by multiplying by independent processes of the same type, then universal behaviour, i.e. that described by Eqn.(7), will be produced[38]. The small scale limit can be taken later; this involves its own difficulties, however these are quite distinct from the question of universality classes. The continuous cascade is built in such a manner by densification, adding more and more intermediate scales in a given multiplicative process.

Thus, since we wish our generator to be stable under addition, we choose it to be a Lévy noise with some parameter α, appropriately weighted and filtered so as to satisfy the other necessary conditions mentioned above. In order to ensure convergence (i.e. to keep K(q) finite for q>0) an extremal asymmetric Lévy variable must be used[27,31,38]. Since the field ε_λ is obtained by exponentiating Γ_λ, which is a sum of these noises (the equivalent of undergoing a multiplicative cascade process), convergence is required.

Multifractals obtained using the Lévy noise generator with parameter α will have the following moment scaling function, K(q), relating the scaling of the moments and the scale:

$$K(q) = \frac{C_1}{\alpha - 1}\left(q^\alpha - q\right) \qquad (8).$$

given that $\alpha \neq 1$, where $0 < \alpha \leq 2$. C_1 is the codimension of the mean of the field, characterizing the sparseness of the mean, and the Lévy index α characterizes the degree of multifractality[31]. As $\alpha \to 0$ K(q) becomes linear and the monofractal β-model[22,23,24,25] is approached; α=2 corresponds to a lognormal model.

We can obtain from this via a Legendre transform the codimension function[31]:

$$c(\gamma) = C_1\left(\frac{\gamma}{C_1\alpha'} + \frac{1}{\alpha}\right)^{\alpha'} \qquad (9)$$

Where $1/\alpha + 1/\alpha' = 1$.

The K(q) has the α-dependence we expect for a Lévy noise, with the linear term arising due to the normalization requirement that $K(1) = 0$. Hence we can determine all the statistical properties of a process using only the two parameters, α and C_1.

For nonconservative fields[28,31], such as density fields f related to ε_λ in a scaling manner ($\langle|\Delta f_\lambda|\rangle = \varepsilon_\lambda \lambda^{-H}$), there is a third fundamental parameter, H, which is a measure of the degree of (scale by scale) non-conservation of the field:

$$\langle|\Delta f_\lambda|\rangle = \lambda^{-H} \qquad (10).$$

The value of H can be determined from the scaling of the power spectrum and the moment scaling function. If necessary, a spectral filter (fractional integration) of the form k^H can be used to transform a non-conservative field into a conservative field. This will be described below. For now, we note that since the energy spectrum E(k) is the Fourier transform of the autocorrelation function (a second order moment), we obtain $E(k) \sim k^{-\beta}$, where

$$\begin{aligned} \beta &= 1 - K(2) \quad \text{(conservative)} \\ \beta &= 1 - K(2) + 2H \quad \text{(non-conservative)} \end{aligned} \qquad (11)$$

We thus see that the parameter H also specifies the degree of statistical non-stationarity ("non-homogeneity") of the field.

If $H \neq 0$, then the universal forms for K(q) and c(γ) are given by:

$$K(q) \to K(q) - qH \qquad (12)$$

and

$$c(\gamma - H) = C_1\left(\frac{\gamma}{C_1\alpha'} + \frac{1}{\alpha}\right)^{\alpha'} \qquad (13)$$

(i.e. $\gamma \to \gamma - H$).

Finally if the parameter α is identically unity then (for all values of H):

$$K(q) - qH = C_1 \cdot q \cdot \log(q)$$

and

$$c(\gamma - H) = C_1 \exp\left(\frac{\gamma}{C_1} - 1\right) \qquad (14)$$

Again as expected. Eq. (14) can be seen to follow from taking the limit as $\alpha \to 1$ of Eqs.(12) and (13) and applying l'Hôpital's rule.

It is worthwhile at this point to note the correspondence between the formalism of universal multifractals and the strange attractor formalism. In the $f(\alpha)$-$\tau(q)$ notation we have the following[32]:

$$\begin{aligned} f_D(\alpha_D) &= D - c(\gamma), \ \alpha_D = D - \gamma \\ \tau_D(q) &= (q-1)D - K(q) \end{aligned} \qquad (15)$$

Parameters for many multifractal fields have been measured. Some of these are tabulated in Table 1.

Field	α	C_1	H	Range of scales	Refs
Clouds Visible	1.35	0.15	0.3	160m→ 4000km	(2)
Clouds Infra Red	1.35	0.15	0.4	160m→ 4000km	(2)
Clouds Microwave	1.60	0.10	0.35	160m→ 4000km	(1)
Rain Radar	1.35	0.30	0.0	30m→ 64km	(2)
Sea Ice (radar)	1.7	0.05	0.0	50m→25km	(10)
Ocean surface (0.95μm)	1.1	0.25	0.35	1m→50m	(5)
Topography	1.8	0.05	0.5	50m→1000km	(4)
Seismicity	1.35	1.9	0.0	1km→500km	(11)
Pollution (Seveso)	1.2	0.8	-0.2	30m→5km	(16)
Raingauges	1.35	0.20	0.0	50km→ 4000km	(2)
Wind windtunnel	1.30	0.25	1/3	1ms→ 1s	(3)
Wind atmosphere	1.45	0.23	1/3	1ms→ 1s	(6)
Temperature	1.20	0.35	0.30	0.1s→ 1000s	(3)
Low frequency speech	2.0	0.1	-.35	0.1s→1000s	(14)
Hadron Jets	0.7	0.6	_	_	(15)
Apparent Galactic Luminosity	1.0	1.0	_	0.3°→5°	(12)

Table 1: Multifractal parameters determined for a variety of fields with the corresponding ranges of scale. The accuracy of most parameters is ~ ±0.1.

3. Simulation

Discrete Cascades

The simulation of a discrete cascade is straightforward. Given that we wish to simulate universal multifractals, i.e. those whose statistics are described by Eqs.(8)-(9), we specify the C_1 and α desired and use the noise that corresponds to this to obtain the generator. We generate unit Lévy variables with parameter α and modify their amplitude by multiplying by the constant $(C_1(\alpha'/\alpha))^{1/\alpha}$ required to obtain the desired C_1. These noises are generated according to the procedure given by Chambers et al[37], who give an expression for the representation of an extremal Lévy-stable variable of index α, $S(\alpha)$:

$$S(\alpha)=\frac{\sin\alpha(\Phi-\Phi_0)}{(\cos\Phi)^{1/\alpha}}\left(\frac{\cos(\Phi-\alpha(\Phi-\Phi_0))}{W}\right)^{(1-\alpha)/\alpha},\alpha\neq 1 \qquad (16)$$

$$S(1)=\frac{2}{\pi}\left(\left(\frac{\pi}{2}-\Phi\right)\tan\Phi+\ln\left(\frac{\pi W\cos\Phi}{\pi-2\Phi}\right)\right) \qquad (17)$$

$$\Phi_0=\frac{\pi}{2}(1-|1-\alpha|)/\alpha \qquad (18)$$

Here, Φ is a uniform random variable on $(-\pi/2,\pi/2)$, and W is a standard exponential deviate, with W and Φ mutually independent. The constant $(C_1(\alpha'/\alpha))^{1/\alpha}$ is needed as the above procedure assumes that the scale parameter is unity. This technique for generating stable random variables necessitates the production of only two random variables and correspondingly few operations upon them, and is thus superior to the slowly converging algorithm given in Wilson[27], which uses the property that Lévy variables are stable regions of attraction to generate them by renormalized sums of many hyperbolic variables with exponent α. Although it is stated that the number of terms, n, in the sum must be very large ($n \approx 30$ for α=1.5 is suggested), further tests have shown that for accurately reproducing K(q) over a reasonable range (e.g. q<5), particularly for α near 2, n is much larger than previously believed[40].

Given a desired scale ratio λ, at each scale Λ from the largest scale to the smallest scale 2^Λ independent noises with the desired parameters are generated These noises, once generated, are then exponentiated to give the multiplicative increments. Each point of the field is then considered to be contained in a specific box at each scale and the field value at that point is given by the product of all the corresponding multiplicative increments. (See Fig.2). The field is then normalized, in keeping with the conservation of the mean condition. To normalize the field, we divide by the expected value of the non-normalized field. This is equal[31] to $\lambda^{C_1/(\alpha-1)}$. It is, in fact, this factor which gives rise to the linear term in q in Eq.(12). This is done rather than dividing by the mean of the specific field produced because we wish conservation only on an ensemble of fields. Conservation holds only on the ensemble average, but will be broken on any particular realization. This is termed canonical conservation.[31,38] Much more restrictive processes involving exact conservation on each realization (called "microcanonical conservation") are also possible, but such processes do not have well-defined universality classes, eliminate the strong singularities, and have properties which depend on the exact details of the construction process including the discrete ratio used to define the microcanonical conservation law.

The disadvantage of using discrete cascades to simulate multifractal fields is that the discrete cascade is nonphysical: energy does not actually cascade in scale steps of factors of two, or of other integer ratio. Also, at least in its usual real-space implementation, it involves straight construction lines which are highly unrealistic: they can result in, for

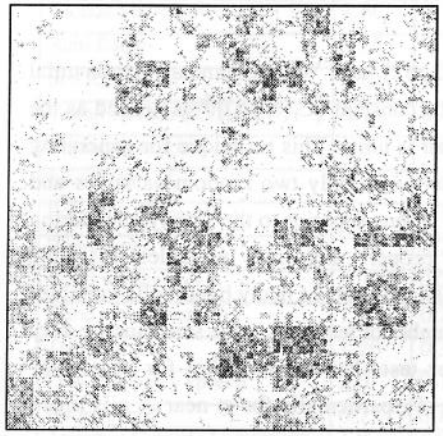

α=2.0, C_1=0.2

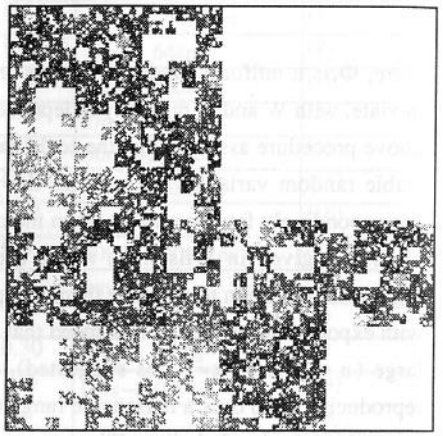

α=0.5, C_1=0.2

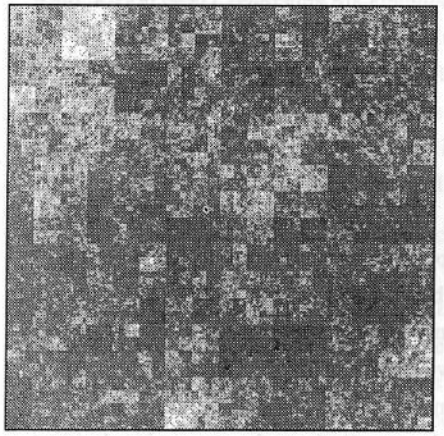

α=2.0, C_1=0.05

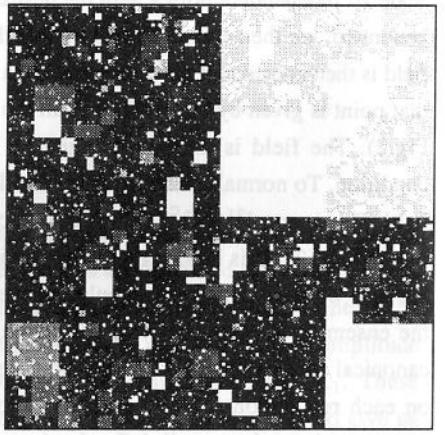

α=0.5, C_1=0.05

Figure 3. Two-dimensional discrete simulations, 256x256. The seed is constant.

example, square clouds. It is necessary to use continuous cascades, obtained by the densification of discrete cascades, to get an idea of what the actual physical process looks like. Examples of discrete cascades are given in Figure 3.

Continuous Cascades

In order to physically simulate the densification of the cascade process, we use Fourier Transform techniques. We therefore look for the Fourier space generator that will satisfy the four conditions laid out previously. We proceed in the following manner:

Given the desired value for α and C_1, we proceed as for a discrete cascade, producing for each grid point a noise $(C_1/(\alpha-1))^{1/\alpha} S(\alpha)$.

In order to weight the noise to obtain a logarithmic divergence of $K_\lambda(q)$, this noise is then Fourier transformed using an FFT. The distinction between a continuous transform and the discrete FFT is taken into account by multiplying by a constant, $\kappa_d(\lambda)$. This is related to the Euler constant correction described elsewhere[27,28]. Taking into account the scale ratio and dimensionality dependence, this constant is just the ratio of the integral to the sum, in d dimensions, over the total scale ratio:

$$\kappa_d(\lambda) = \frac{\int_1^\lambda k^{-d} d^d k}{\sum_1^\lambda \frac{1}{k^d}} \qquad (19)$$

We now wish to obtain the 1/f-noise spectrum, to give multiscaling behaviour. To do this it is necessary to weight the Fourier transform of the Lévy noise. The correct weighting factor can be determined by considering the property of a Lévy random variable[36], $S(\alpha)$:

$$\langle \exp(qS(\alpha)) \rangle = \exp(q^\alpha) \qquad (20)$$

This property requires that, to achieve a spectrum of k^{-1}, a weighting factor[31] of $w(\mathbf{x}) \propto |\mathbf{x}|^{-d/\alpha}$ is needed for the real-space noise $S(\alpha,\mathbf{x})$; this corresponds to a factor of $w(\mathbf{k}) \propto |\mathbf{k}|^{-d/\alpha'}$ in k-space. In addition, the noise is band-limited by filtering out all noises except those concentrated in the band with wave-number between 1 and λ, using a filtering function $f(\lambda,\mathbf{k})$. This yields for the generator

$$\Gamma_\lambda = \mathcal{F}^{-1}\left\{ \left(\frac{C_1}{\alpha-1}\right)^{1/\alpha} \tilde{S}(\alpha,\mathbf{k}) |\mathbf{k}|^{-d/\alpha'} f(\lambda,\mathbf{k}) \kappa_d(\lambda) \right\} \qquad (21)$$

($\mathcal{F}^{-1}$ represents the inverse Fourier transform). The function $f(\lambda,\mathbf{k})$ is chosen to be one for $|\mathbf{k}| \le \lambda$, and decaying exponentially for $|\mathbf{k}| > \lambda$. This is in order to filter out wave numbers greater than λ (as required by condition 2). Since sharp cutoffs (δ-functions or

step functions) in Fourier space cause real-space sine wave "ringing" effects, an exponential decay is used. This adds negligibly (less than 1%) to the constant $\kappa_d(\lambda)$ for $\lambda > 128$. However, if desired, this factor can be taken into account by the appropriate modification of Eqn.(19)

Finally, the weighted noise is transformed back into real space and is exponentiated to give the required field ε_λ. It is also normalized by dividing by the expected value of the field (i.e. $\lambda^{C_1/(\alpha-1)}$) to satisfy condition 4, following the process described in the discrete cascade section.

Examples of continuous cascades in one dimension are given in Figures 4-7 and 12-13. These simulations are over a scale ratio of 256 (extending this to larger ranges rapidly increases the variability of the field, resulting in a field that is difficult to visualize). Computationally, it is not difficult to extend this to much larger fields, depending on the computing power available—on a Silicon Graphics IRIS 4D/35, the generation of 100 one-dimensional simulations with $\lambda=2^{14}$ will take on the order of 8 minutes. For very large sizes the limiting factor is not so much the computation time but the memory requirements of an array of the size of the field.

Fig.4 shows a series of simulations for C_1=0.9 and varying values of α. The fields are vertically offset from each other. As α decreases, the high values of the field do not dominate as much as for larger values of α; there are more large deviations from the mean, as we expect for the "thick" tail of the probability distribution. In the case where C_1=0.01 (Fig 5), the fields are typically at values near 1, with spikes in both directions. The fields with higher values of α are seen to have a more symmetric distribution of deviations from the mean. Since C_1 is so small, the fields are nearly space-filling. This is seen particularly for α=1.04, where the field is nearly uniform in comparison to higher α-values and there are primarily regularities (i.e. downward spikes). This is evidence of the fact that as α decreases, the Lévy noise in fact becomes asymmetric with only negative hyperbolic jumps, i.e. "Lévy holes"[31]. When the field is renormalized, the lowest values are "washed out". This is most obvious when C_1 is small.

Figures 6 and 7 show series of one dimensional simulations with fixed α and varying C_1. It is apparent from them that C_1 is the measure of the sparseness of the field: the higher the C_1, the fewer the field values corresponding to any given singularity. (Because the field is normalized, the spikes appear higher for the fields with higher C_1). It is also again apparent that the higher α fields are dominated by a few large singularities.

Examples of two-dimensional continuous cascade simulations are given in Colour Illustrations 1-3. These fields have been k^{-H}-filtered for easier recognition of the salient features. The three-dimensional representation of some of these fields are given in Figures

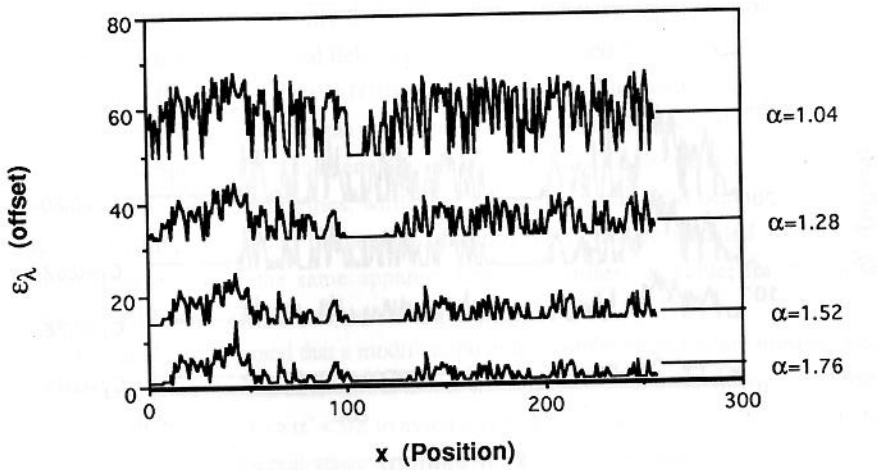

Figure 4. One-dimensional simulation of length 256, with C_1=0.9 and varying α. These simulations have been vertically offset so as not to overlap.

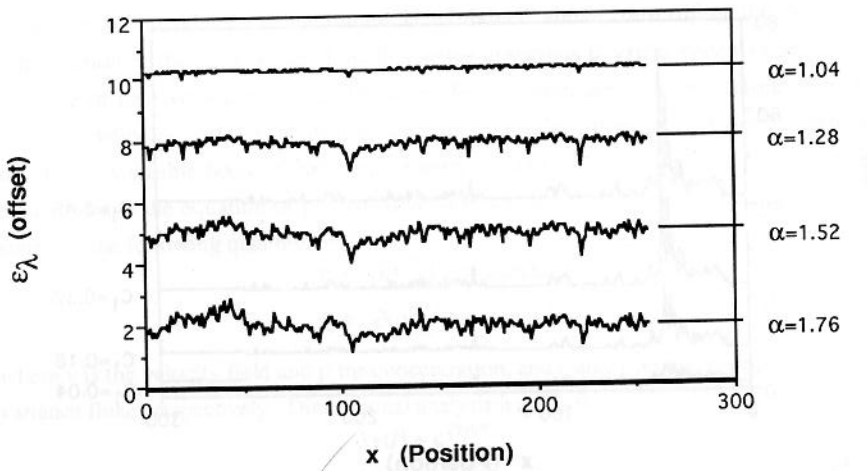

Figure 5. One-dimensional simulation of length 256, with C_1=0.01 and varying α. These simulations have been vertically offset so as not to overlap.

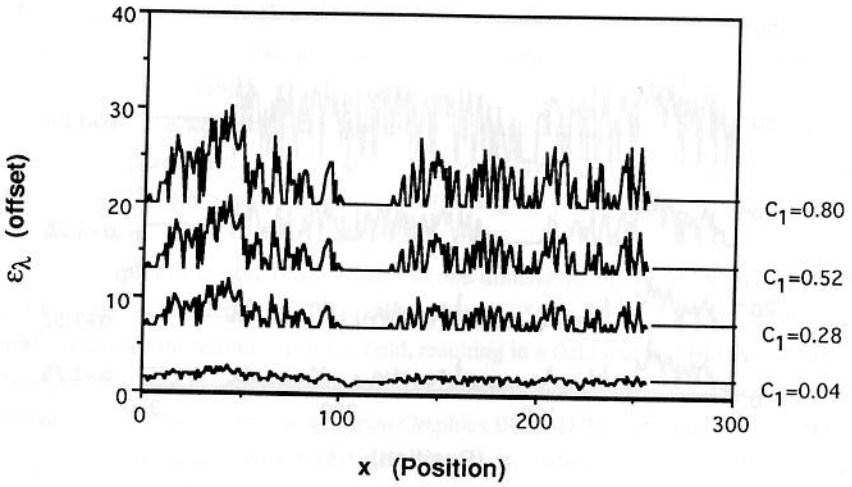

Figure 6. One-dimensional simulation of length 256, with α=1.4 and varying C_1. These simulations have been vertically offset so as not to overlap.

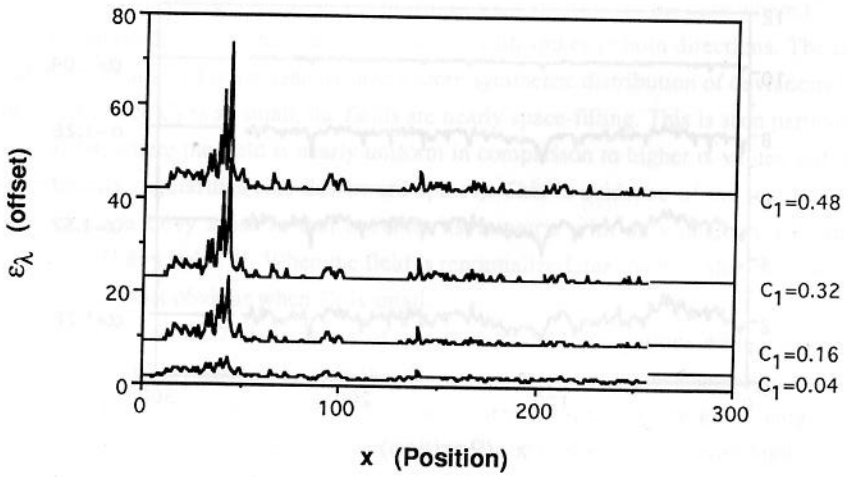

Figure 7. One-dimensional simulation of length 256, with α=2.0 and varying C_1. These simulations have been vertically offset so as not to overlap.

8-11. The same features can be noted for the differing values of α and C_1. The fields with higher values of α are generally dominated by a few areas with upward spikes (i.e. singularities); the lower α-valued fields have more high-valued singularities. The degree of sparseness that C_1 characterizes is fairly obvious from the illustrations. (Although recall that after filtering C_1 is no longer the codimension of the mean of the visualized field, it still provides a description of the sparseness). For higher C_1, the fields are sparsely scattered, with only a few large singularities, while as C_1 is reduced, the field becomes more and more space-filling. Note that in these illustrations the fields are rescaled so that their maximum values are at the same apparent height regardless of value; for the colour illustrations all colours are given by actual field value.

It should also be noted that a modification in the simulation procedure must be made for fields with $\alpha < 1$. In this case, direct use of the factor $w(\mathbf{k}) \propto |\mathbf{k}|^{-d/\alpha'}$ leads to numerical overflow (recall that $\alpha < 1 \Rightarrow \alpha' < 0$); to avoid this problem it suffices to filter by using the numerical transform of the real-space term $w(\mathbf{x}) \propto |\mathbf{x}|^{-d/\alpha}$. The remainder of the simulation program proceeds as above.

4. Fractional Integration and Non–Conservative Quantities

In order to simulate certain physical fields, for example clouds, or galaxies, it is necessary to introduce the parameter H explained above, describing the degree of conservation of the field. To see how this arises in various physical systems consider the example of passive scalar clouds, i.e. cloud fields which are passively advected by the turbulent velocity without themselves affecting the latter; these obey Corrsin-Obukhov scaling[41]. A sizable body of turbulence theory exists for these. From the Navier-Stokes equations and the equation of passive advection we find that the nonlinear terms exactly conserve the following quantities[28]:

$$\varepsilon = -\partial\langle \mathbf{v}^2 \rangle / \partial t = \text{constant}$$
$$\chi = -\partial\langle \rho^2 \rangle / \partial t = \text{constant} \qquad (22)$$

where $\mathbf{v}$ is the velocity field and ρ the concentration, and ε and χ are the energy and scalar variance fluxes respectively . Dimensional analysis implies that

$$\Delta v(l) \approx \varepsilon^{1/3} l^{1/3}$$
$$\Delta \rho(l) \approx \varphi^{1/3} l^{1/3} \qquad (23)$$
$$\text{where } \varphi = \chi^{3/2} \varepsilon^{-1/2}$$

A passive scalar cloud therefore already involves two nonlinearly coupled cascade processes, for ε and χ; in general we will need to use vector cascade processes, using the

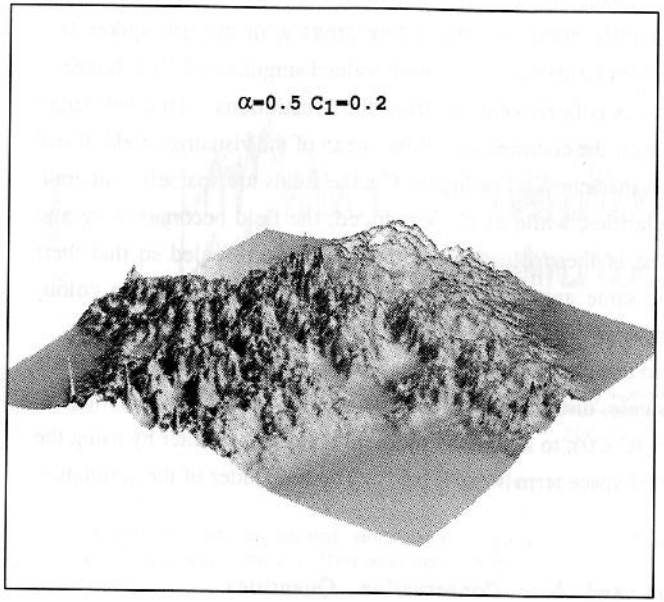

Figure 8. 3–D representations of 256x256 simulated fields.

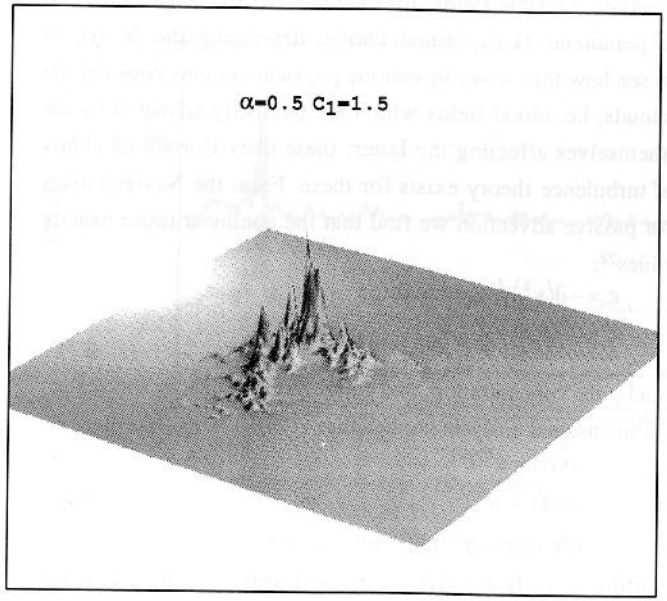

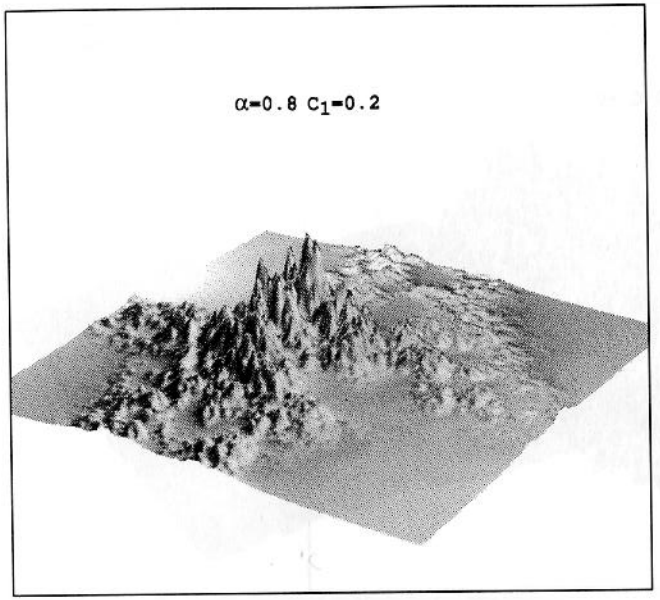

Figure 9. 3–D representations of 256x256 simulated fields.

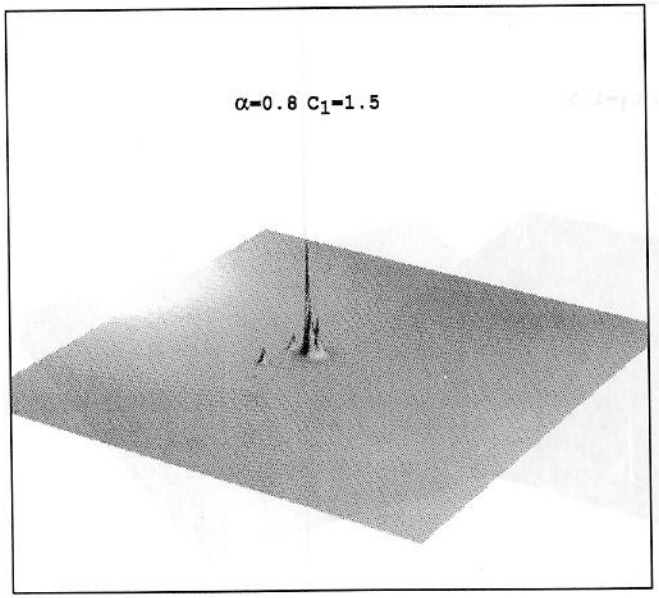

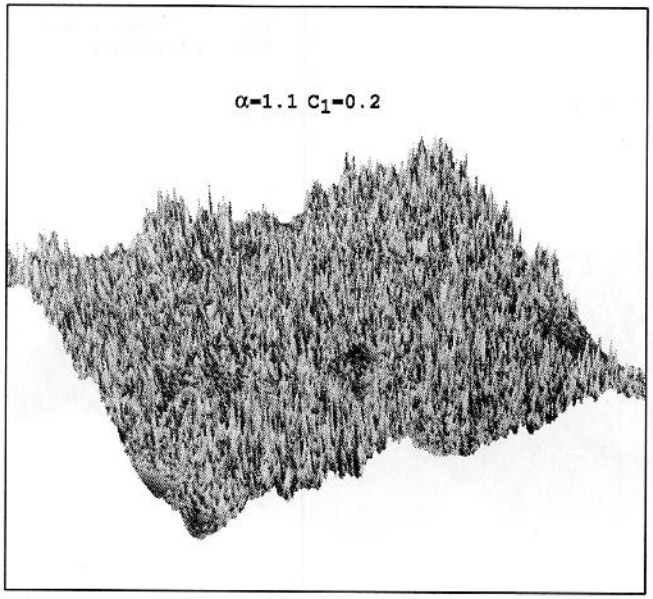

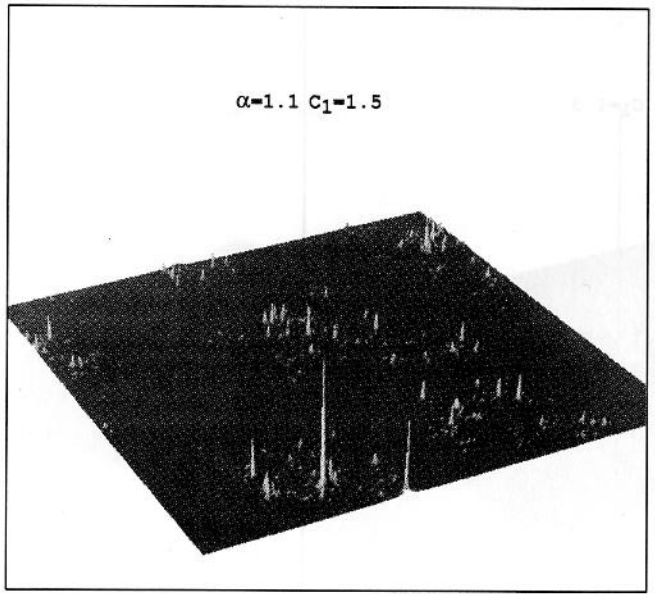

Figure 10. 3–D representations of 256x256 simulated fields.

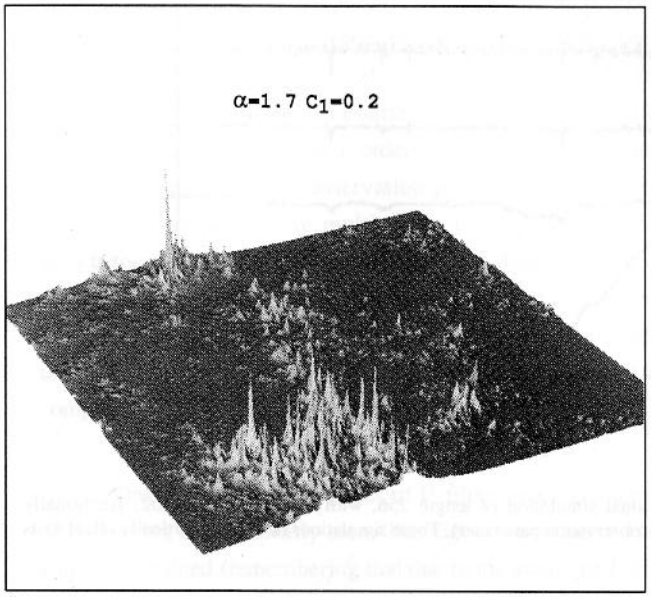

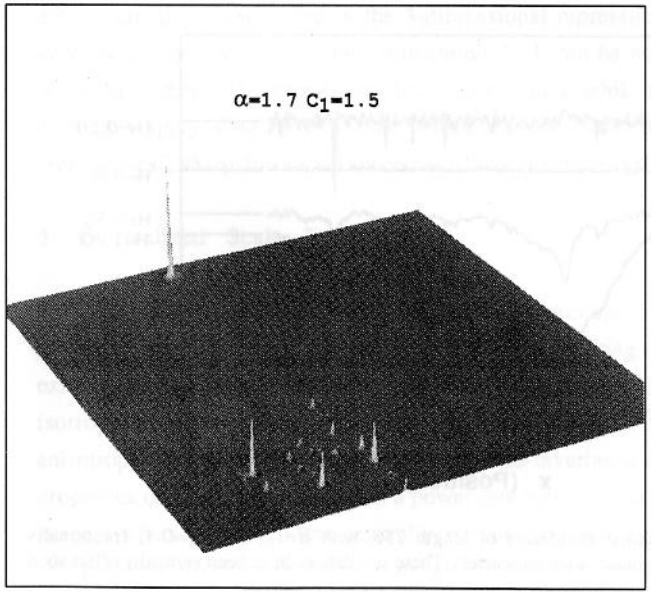

Figure 11. 3–D representations of 256x256 simulated fields.

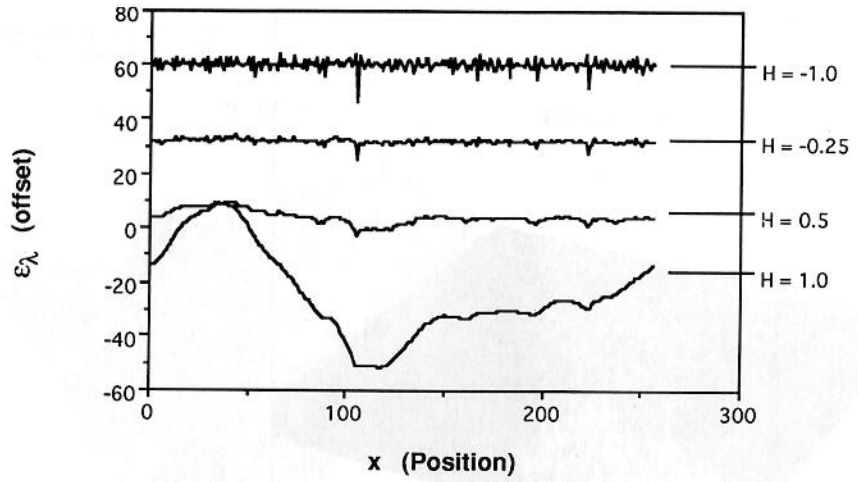

Figure 12. One-dimensional simulation of length 256, with α=1.8 and C_1=0.02, fractionally integrated with varying H (non-conservation parameter). These simulations have been vertically offset so as not to overlap.

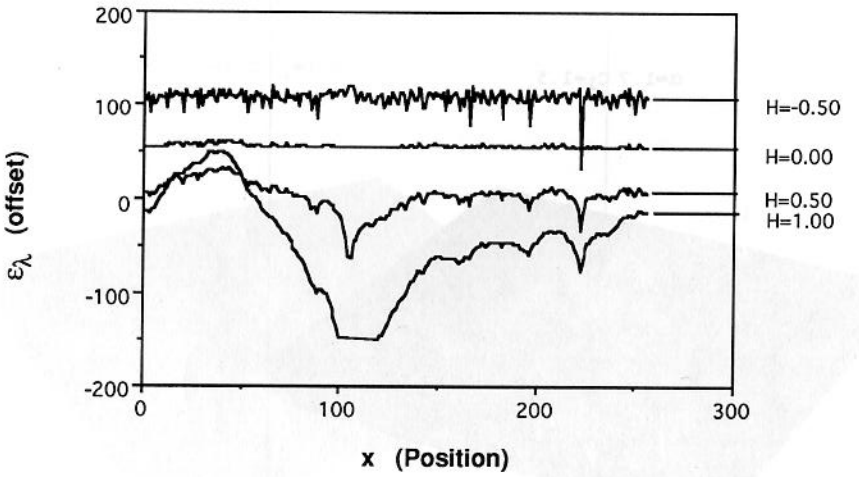

Figure 13. One-dimensional simulation of length 256, with α=1.5 and C_1=0.4, fractionally integrated with varying H (non-conservation parameter). These simulations have been vertically offset so as not to overlap.

new formalism of "Lie cascades"[42]. Here, we make the simplest assumption, that χ is completely statistically dependent on ε. The field ρ therefore satisfies $\Delta\rho \approx \varepsilon^{1/3} l^{1/3}$. The cube-root of the conserved field is easy to calculate. To introduce the $l^{1/3}$ factor, we transform the field back into Fourier space and multiply it by the factor $k^{-1/3}$. This is in effect a fractional integration of order[31] 1/3. It results in a scale-invariant smoothing of the field. For a general non-conservation parameter H, the simulated conservative field is fractionally integrated by multiplying in k-space by k^{-H}. For H>0, this results in a smoothing of the field; H<0 corresponds to a differentiation and leads to a roughening of the field. It must also be noted that, since the factor k^{-H} will become infinite for positive H as $k \to 0$, the term (corresponding to the mean of the field) cannot be fractionally integrated using Fourier techniques[31]; it must be integrated seperately in real space. The k=0 component $\bar{\varepsilon}$ of a simulation of linear size L is obtained by the following multiplication :

$$\bar{\varepsilon} \to \bar{\varepsilon}\left(L^H\right) \tag{24}$$

One-dimensional examples of H-filtering are given in Figs 12 and 13. The effects of H-filtering can be clearly seen. The higher the value of H used, the smoother the field which is obtained (remembering that due to the scale, the H-filtered fields are increased in size relative to the normalized conservative field). On the other hand, negative values of H accentuate the singularities already present in the field. The smoothing and roughening effects are also clearly seen in the 3-dimensional representation of a two dimensional continuous cascade. (See Colour Illustration 4). It can be noted that the smaller spikes, when sufficiently H-filtered, are almost eliminated, while for negative H, the field is extremely spiky. One can also note that negative values of H lead to the production of "regularities", sharp downward spikes, as is expected for a differentiation of the field.

5. Generalized Scale Invariance

A multifractal field is developed from a process that is scale-invariant. In its simplest form, this scale-invariance is isotropic; the resulting multifractals are self-similar, exhibiting no preferred direction in space. However, geophysical fields are seldom, if ever, isotropic. Preferred directions associated with texture and morphology exist whose anisotropy often varies with scale. Isotropic scale-invariance indicates that the (statistical) properties of a field are changed in a power-law way with an isotropic change in scale of space, such as zooming. More generally, we can consider a system to be scale-invariant if this property remains true under more general nonisotropic scale changes. That is, there

exists a scale changing operator[31,43] for a given scale ratio λ, T_λ, such that given balls B_λ at this scale ratio,

$$T_\lambda B_1 = B_\lambda \tag{25}$$

T_λ is the rule relating the statistical properties at one scale to another and involves only the scale ratio (there is no characteristic "size"), so that $\mathbf{x}_\lambda = T_\lambda \mathbf{x}_1$, where $\mathbf{x}_\lambda$ and $\mathbf{x}_1$ are vectors on B_λ and B_1 respectively. This implies that T_λ has certain properties. In particular, if and only if $\lambda_1\lambda_2 = \lambda$, then

$$B_\lambda = T_{\lambda_1} B_{\lambda_2} = T_{\lambda_2} B_{\lambda_1}, \tag{26}$$

i.e., T_λ has the group properties:

$$T_{\lambda_2} T_{\lambda_1} B_1 = B_\lambda = T_{\lambda_1} T_{\lambda_2} B_1 \tag{27}$$

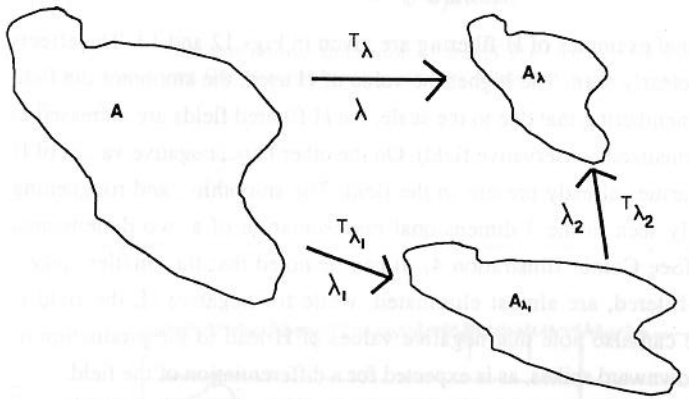

Figure 14—Illustration of the group property of the scale changing operator.(18)

In generalized scale invariance (GSI), T_λ, the scale-changing operator, can be much more general than the standard isotropic dilation. As indicated earlier, in general, a scale invariant system will be one in which the small and large scales are related by a scale changing operation that involves only the scale ratios; there is no characteristic size. Following the development of Schertzer and Lovejoy[43], we note that to be completely defined, GSI needs more than a scale changing operator; it also requires a definition of the unit scale, as well as a definition of how to measure the scale. These three basic elements can be summarized as follows:

i) The unit ball B_1 which defines all the unit vectors. If an isotropic ball (*i.e.*, circle or sphere) exists, we call the corresponding scale the "spheroscale".

ii) The scale changing operator T_λ which transforms the scale of vectors by scale ratio λ. T_λ is a one parameter multiplicative group $\Rightarrow T_\lambda = \lambda^{-G}$, where G is the generator of the group.

If G is an n x n matrix and $\mathbf{x}$ is an n-dimensional vector then we may use:

$$\lambda^{-G} = \exp\left(-G\cdot\ln(\lambda)\right) = 1 - G\cdot\ln(\lambda) + \frac{1}{2}G^2\cdot\ln^2(\lambda) - \cdots . \tag{28}$$

This is linear GSI[44]. When G is a more general (*i.e.*, nonlinear) generator, we must define λ^{-G} by differential equations using the fact that G defines infinitesimal transformations.

iii) A measure of scale such as some power of the volume of B_λ ; the exact definition is somewhat a matter of convenience or convention.

The simplest type of scaling is self-similar scaling, as in isotropic cascades. Here, $T_\lambda = \lambda^{-1}\mathbf{1} \Rightarrow G = \mathbf{1}$, where $\mathbf{1}$ is the identity matrix. Taking B_1 as the unit circle, the balls B_λ are circles.

A more interesting case occurs when the scaling is different in two (or more) fixed directions, *e.g.*, coordinate axes. This type of scaling is called "self-affine": G is a diagonal matrix. A simple example is an anisotropic scaling model of atmospheric stratification, which provided the initial impetus for developing GSI[29,30]. Consider a vertical cross-section of the atmosphere (see figure 16), using

$$G = \begin{bmatrix} 1 & 0 \\ 0 & H_z \end{bmatrix} \text{ and } \mathbf{x} = \begin{bmatrix} x \\ z \end{bmatrix}, \tag{29}$$

where x is the horizontal distance and z is the vertical distance. Then the relation $\mathbf{x}_\lambda = T_\lambda \mathbf{x}_1$, where $\mathbf{x}_1$ is the position vector of the unit ball (a circle in this case), becomes

$$\begin{bmatrix} x_\lambda \\ z_\lambda \end{bmatrix} = \lambda^{-\begin{bmatrix} 1 & 0 \\ 0 & H_z \end{bmatrix}} \cdot \begin{bmatrix} x_1 \\ z_1 \end{bmatrix} = \begin{bmatrix} \lambda^{-1} & 0 \\ 0 & \lambda^{-H_z} \end{bmatrix} \cdot \begin{bmatrix} x_1 \\ z_1 \end{bmatrix} = \begin{bmatrix} \lambda^{-1}\cdot x_1 \\ \lambda^{-H_z}\cdot z_1 \end{bmatrix}. \tag{30}$$

When $\lambda \gg 1$, then the cells are strongly vertically aligned. Defining the unit vectors $\mathbf{x}_1$ as circles, this corresponds to structures (*e.g.*, clouds) whose average cross-sections are circular—this is the "spheroscale". When $\lambda \ll 1$, they are horizontally flat.

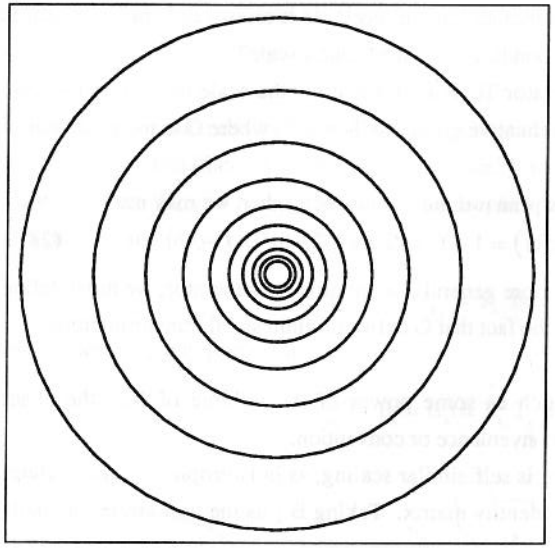

Figure 15—Self-similar scaling.

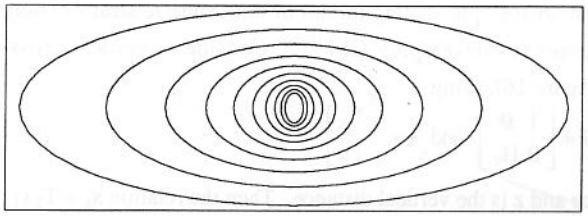

Figure 16—Self-affine scaling with $H_z = 5/9$. The shape of the balls models the average eddy shape; the flattening of the large balls models the fact that the atmosphere is increasingly stratified at large scale, and the small-scale vertically oriented balls correspond to "convective" cells or "rain shafts"

Figure 16 shows an example of a deterministic self-affine fractal set. As expected, the structures which are initially horizontally flat at large scales become more and more vertically flat at small scales.

One might also expect differential rotation (e.g. associated with Coriolis force in the atmosphere for clouds). This can be modeled by a matrix G with off-diagonal elements. We decompose G into quaternion-like elements[29,45]:

$$G = d\mathbf{1} + e\mathbf{I} + f\mathbf{J} + c\mathbf{K},$$

where

$$\mathbf{1} = \begin{bmatrix} 1 & 0 \\ 0 & 1 \end{bmatrix}, \quad \mathbf{I} = \begin{bmatrix} 0 & -1 \\ 1 & 0 \end{bmatrix}, \tag{31}$$

$$\mathbf{J} = \begin{bmatrix} 0 & 1 \\ 1 & 0 \end{bmatrix}, \quad \mathbf{K} = \begin{bmatrix} -1 & 0 \\ 0 & 1 \end{bmatrix}.$$

To obtain $\lambda^{-G} = e^{-G\ln\lambda}$, we use the series expansion of the exponential function with the following identities:

$$(G - d\mathbf{1})^{2n} = (e\mathbf{I} + f\mathbf{J} + c\mathbf{K})^{2n} = a^{2n}\mathbf{1}, \tag{32}$$

$$(G - d\mathbf{1})^{2n+1} = a^{2n}(G - d\mathbf{1}), \tag{33}$$

where n is an integer and $a^2 = c^2 + f^2 - e^2$. Writing[29,45] $U = \ln\lambda$:

$$T_\lambda = \lambda^{-G} = \lambda^{-d}\lambda^{(G-d\mathbf{1})} = \lambda^{-d}\left[\mathbf{1}\cosh(aU) - (G - d\mathbf{1})\frac{\sinh(aU)}{a}\right] \tag{34}$$

When $a^2<0$, the above formula holds but with $|a|$ replacing a and ordinary trigonometric functions rather than hyperbolic functions. The case $a^2>0$ corresponds to domination by stratification, whereas $a^2<0$ to domination by rotation.

The application of GSI to simulations is an important one; most geophysical fields include some element of anisotropy, such as gravitation and the Coriolis effect of the earth's rotation in the case of the atmosphere, or, in the case of earthquakes, preferred direction along the faultline. In addition, GSI has been used in the simulation of galaxies[43]; rotation dominance leads to spiral galaxy shapes, while stratification dominance tends to lead toward barred galaxy shapes.

Simulation of GSI

In order to model the effects of GSI, it is necessary to make some changes in the steps explained above. Rather than the usual dimension, we now use the elliptical dimension, given by d_{el}=Tr G, the trace of the GSI matrix. The volume of the balls B_λ varies as $\lambda^{-d_{el}}$, so it is necessary to replace d by d_{el}. In addition, the weighting factor $w(\mathbf{k}) \propto |\mathbf{k}|^{-d/\alpha'}$ that determines the multi-scaling is changed not only by this replacement. It also becomes necessary to replace the modulus $|\mathbf{k}|$ by $\lambda(\mathbf{k})$. All the filters must be appropriately anisotropic.

In order to determine $\lambda(\mathbf{k})$, we consider GSI in Fourier space. Given $\mathbf{x}_\lambda = T_\lambda\mathbf{x}_1$, we wish to determine the Fourier space operator $\tilde{T}_\lambda$ such that $\mathbf{k}_\lambda = \tilde{T}_\lambda\mathbf{k}_1$ (corresponding to T_λ). In fact, by assuming the existence of matrices G and $\tilde{G}$ that generate the scale changing operators (with $T_\lambda = \lambda^{-G}$ and $\tilde{T}_\lambda = \lambda^{-\tilde{G}}$), and requiring invariance of the scalar product

under scale changes, it can be shown[44,45] that $\tilde{G}=G^T$. It remains to solve for the scale λ from the equation $\mathbf{k}_\lambda = \tilde{T}_\lambda \mathbf{k}_1$, i.e. to find λ such that $\mathbf{k}_1 = \tilde{T}_\lambda^{-1}\mathbf{k}_\lambda$; when $\mathbf{k}_1$ is on the unit circle, this requires $\left|\tilde{T}_\lambda^{-1}\mathbf{k}_\lambda\right| = 1$. To solve this, we need in addition a definition of the unit ball, i.e. some $U_1=\ln\lambda_1$ that defines the spheroscale. Given this, in two dimensions the scale λ can be found. Eq.(34) is used to determine $\tilde{T}_\lambda$ and the equation $\mathbf{k}_\lambda = \tilde{T}_\lambda \mathbf{k}_1$ is expanded to yield the following transcendental equation[44]:

$$\begin{aligned}
&\ln(P\cosh^2(a(U-U_1))+Q\sinh^2(a(U-U_1))-R(\sinh(2a(U-U_1)))=2U\\
&P=k_x^2+k_y^2\\
&Q=\frac{k_x^2(c^2+(f-e)^2)+k_y^2(c^2+(f+e)^2)+4k_xk_yce}{a^2}\\
&R=\frac{(k_x^2-k_y^2)c+2k_xk_yf}{a}\\
&U=\ln\lambda
\end{aligned} \qquad (35)$$

This equation is then solved for λ for each value of k_x and k_y, and this value is then used in place of k in the weighting function $w(\mathbf{k})$. The same must be done for the k^{-H} filtering if the field is to be fractionally integrated. By examining Colour Illustration 5, the effects of different GSI parameters can be seen. Altering the matrix G to produce rotation- or stratification-dominant fields noticeably changes the texture of the resulting simulation. Stratification dominant fields will have structures smaller than the spheroscale compressed in the direction of stratification, while structures larger than the spheroscale will be stretched in that direction. The total rotation as λ is increased from 1 to ∞ is less than $\pi/2$. Rotation-dominant fields are differentially rotated; the orientation of the large-scale structures is rotated with respect to the smaller-scale ones, an infinite number of rotations as λ is increased from 1 to ∞. Some stratification is useful to make this clearer.

In addition, the size of the spheroscale plays an important role in determining the nature of the resulting field. A very large spheroscale (Fourier space: this is small in real space) combined with stratification, for example, will result in a great deal of "streakiness" at the large scale in real space, since the spheroscale in real space will be at the small scales: these will be isotropic. On the other hand, with a spheroscale midway between the largest and smallest scales, stratification will be seen in opposite directions at the large and small scales in the resulting field.

Simulations can also be made where there is no spheroscale. In this case, a function describing some scale of the desired simulation must be described. Pflug[44] and Lovejoy[46] use the first three symmetric terms of a Fourier expansion to describe $r(\theta)$, i.e. $r(\theta)=r_0+a_1\sin(2\theta)+a_2\sin(4\theta)+b_1\cos(2\theta)+b_2\cos(4\theta)$. (The Fourier transform of a real field respects the symmetry $F(\mathbf{k})=F^*(-\mathbf{k})$ hence we require $r(\theta)=r(\pi-\theta)$). The scale at which this function is described must be given, and care must be taken that the operation of scale-changing on the given function does not result in an overlapping of scales. (That is, within the range of scales in question the scale-changing operator acting on this $r(\theta)$ function gives a single-valued answer: the definition of scale must be unique). Other methods of defining groups of functions closed under scale-changing are currently being examined. Examples of GSI without spheroscales are shown in Colour Illustration 5. Many different textures are possible with the use of non-spheroscale GSI.

6. Conclusions

Scale invariance seems to be a property common not only to complex geophysical fields, but to aspects of biology and astrophysics as well. In the absence of any symmetry-breaking mechanism, scale invariance will be preserved, and even given the breaking of certain symmetries, anisotropic scale invariance may be preserved. We have examined how quite general assumptions concerning scale invariance lead to the idea of multifractals, and how nonlinear "mixing" (including densification) of multiplicative cascade processes leads to the production of universal multifractal fields. The empirically estimated parameters for many of these fields have been tabulated.

Simulations are an invaluable tool in the comprehension of multifractals, and in their use as physical models. Physical processes on multifractals which have already been explicitly considered with the help of such models include the radiative and diffusive transport on multifractals[47], the electromagnetic scattering properties[48], and the sampling and averaging properties of sparse measures[47]. We have described how to simulate both discrete cascades and the more physically relevant continuous cascade, for a general dimension of space. Several points mentioned in earlier papers have been clarified and the ideas expanded upon. In addition, the production of non-conservative fields by scale-invariant roughening or smoothing has been discussed. This allows generation of fields such as topography and the passive scalar cloud field.

Finally, the use of generalized scale invariance in the production of anisotropic cascades has been discussed. Many physical systems show a preferred direction, and the use of GSI allows the simulation of such effects as differential rotation and stratification in directions which can be functions of scale and position. As well, this framework can be used for the generation of time-series and forecasts, where the space-time transformation is not necessarily an isotropic one.

Further work is necessary in a number of areas to increase the utility of simulations. Higher dimensional GSI is very involved and the simulation of three-dimensional and higher dimensioned fields is not currently possible except for special cases. Additionally, techniques for simulating non-linear GSI, which can only be locally approximated by matrices, are lacking. All of these techniques will also be extended to more general fields of vector quantities, through the use of Lie cascades[42]. Applications of the simulation of universal multifractals are also being developed, including methods for forecasting time evolution of rain and cloud fields as well as prediction of earthquakes, and models of radiative transfer in clouds.

7. References

1. D. Lavallée,D. Jourdan, C. Gautier, C. Hooge, *J. Geophys. Res.* (1993) (in press)
2. Y. Tessier, S. Lovejoy, D. Schertzer, *J. Appl. Meteor.* **32.** (1993) p.223-250.
3. F. Schmitt, D. Lavallée, D. Schertzer, S. Lovejoy, *Phys. Rev. Lett.*, **68** (1992) p305-308.
4. D. Lavallée, in *Fractals in Geography,* eds. L. De Cola and N. Lam (Prentice and Hall) p.171-205.
5. Y. Tessier, S. Lovejoy, D. Schertzer, D. Lavallée, B. Kerman , *Geophys. Res. Lett.* (1993) (in press).
6. F. Schmitt, D. Schertzer, S. Lovejoy, D. Lavallée, *Physics of Fluids* (1993) (submitted 9/92)
7. Y.Y. Kagan, and L. Knopoff, *Geophysical Journal R. Astron. Sci.* **62** (1980) p 303.
8. J. Key and A. S. McLaren, *Geophysical Research Letters*, **18** (1991) p.1437
9. B. T. Jones, V. J. Martinez, E. Saar, J. Einasto *Astrophysical Journal* **332. L1.**(Sept 1988)
10. F. Francis, S. Lovejoy, B. Kerman, D. Schertzer, *Geophysical Research Letters* (submitted).
11. C. Hooge, M.Sc. Thesis, McGill University, Montréal, Québec (1993)
12. P. Garrido, M.Sc. Thesis, McGill University, Montréal, Québec (1993)
13. M. Dogterom and L. Pietronero, *Physica* **A171** (1991) p.239.
14. C. Larnder, N. DeSaulnier-Soucy, S. Lovejoy, D. Schertzer, C. Braun, D. Lavallée,*International Journal of Bifurcation and Chaos,* **2** (1992) p.715
15. S. P. Ratti, G. Salvadori, G. Gianini, S. Lovejoy, D. Schertzer, *Proc. of 21st Int. Symp. on Multiparticle dynamics* (Wuhan,1991)
16. G. Salvadori, S. P. Ratti, G. Belli, S. Lovejoy, D. Schertzer, *J. of Toxicological and Environ. Chem.* (1993) (in press).
17. S. Lovejoy, *20th conf. on radar meteorology* (AMS Boston, 1981) p.476
18. S. Lovejoy, B. Mandelbrot, *Tellus*, **37A** (1985) p.209
19. R. Voss, *Proceedings, Siggraph. Conf.* (Detroit, 1983) p.1
20. A. Fournier, D. Fussel, L. Carpenter, *Comm. of the ACM,* **6** (1982) p.371
21. M. Barnsley, *Fractals Everywhere* (Academic Press, San Diego, 1988)
22. E. A. Novikov, R. Stewart, *Izv. Akad. Nauk. SSSR, Ser. Geofiz.*, **3** (1964) p.408
23. A. M. Yaglom, *Dokl. Akad. Nauk. SSSR,* **2** (1966) p.26
24. B. Mandelbrot, *J. Fluid. Mech.*, **62** (1974) p.331
25. U. Frisch, P. L. Sulem, M. Nelkin, *J. Fluid. Mech.*, **87** (1978) p.719
26. D. Schertzer, S. Lovejoy, *Proceedings, 4th Symp. of Turbulent Shear Flows,* 11.1, 11.8
27. J. Wilson, D. Schertzer, S. Lovejoy, in *Non-Linear Variability in Geophysics: Scaling and Fractals,* eds. D. Schertzer and S. Lovejoy (Kluwer, Norwell, MA, 1991), p.183-207
28. D. Schertzer, S. Lovejoy, *J. Geophys. Res.*, **92** (1987) p.9692
29. S. Lovejoy, D. Schertzer,*Water Resources Research,* **21,8** (1985) p.1233
30. D. Schertzer, S. Lovejoy, *P.C.H. Journal,* **6** (1985) p.623
31. D. Schertzer and S. Lovejoy, in*Non-Linear Variability in Geophysics: Scaling and Fractals*, eds. D. Schertzer and S. Lovejoy (Kluwer, Norwell, MA,1991) p.41
32. S. Lovejoy, D. Schertzer, *Multifractals in Geophysics,* Course Notes (AGU-CGU-MSA Spring Meeting, May 11, 1992)
33. D. Schertzer, S. Lovejoy, *Physica* **A 185** (1992) p.187
34. G. Batchelor, A. Townsend, *Proc. Roy. Meteor. Soc.*, **A199** (1949) p.238
35. D. Schertzer, S. Lovejoy in*Turbulent Shear Flows 4,* ed. L. Bradbury, F. Durst, B. Launder, F. Schmidt, J. Whitelaw (Springer-Verlag, Berlin, 1985) p.7
36. W. Feller, *An Introduction to Probability Theory and its Applications, 2nd Ed.* (John Wiley & Sons, New York, 1971)
37. J. M. Chambers, C. L. Mallows, and B. W. Stuck, *Journal of the American Statistical Association,* **71** (1976) p.340
38. D. Schertzer, S. Lovejoy, D. Lavallée, F. Schmidt in *Nonlinear Dynamics of Structures*, ed. R. Z. Sagdeev, U. Frisch, A. S. Moiseev, A. Erokhin (World Scientific,1991), p.213-235

39. B. Mandelbrot, in *Fractals in Geophysics,* ed. C. H. Scholz, B. Mandelbrot (Birkhäuser Verlag, 1989) p.5

40. Brian Watson, private communication

41. A. Obukhov, *J. Geophys. Res.* **67** (1962) p.3011

42. D. Schertzer, S. Lovejoy, in *Space-time Variability and Interdependence for Various Hydrological Processes,* ed. G. Kovaks (U. Press, Cambridge, 1993) (in press)

43. D. Schertzer and S. Lovejoy, *PAGEOPH*, **130** (1989) p.57

44. K. Pflug, Master's Thesis, McGill University, Montréal, Québec (1991)

45. K. Pflug, S. Lovejoy and D. Schertzer, in *Nonlinear Dynamics of Structures*, ed. R. Z. Sagdeev, U. Frisch, A. S. Moiseev, A. Erokhin (World Scientific,1991), p.72-78

46. S. Lovejoy, D. Schertzer, K. Pflug, *Physica* **A 185** (1992) p.121

47. A. Davis, S. Lovejoy, D. Schertzer, *SPIE* **1558** (1991) p.37

48. M. Duncan, S. Lovejoy, F. Fabry, D. Schertzer, *Proc. 2nd Inter. Symp. on Hydro. Appl. of Weather Radar* (U. of Hanover, Sept. 7-10, 1992)

image #	α	C_1	H	G matrix	u_1,spheroscale	r_0, a_1, b_1, a_2, b_2 (see text)
1	1.7	0.1	0.5	$\begin{pmatrix} 1.20 & 0.05 \\ -0.05 & 0.60 \end{pmatrix}$	$u_1 = \ln 100$	-
2	1.7	0.1	0.5	$\begin{pmatrix} 1.00 & 0.40 \\ -0.30 & 0.80 \end{pmatrix}$	$u_1 = \ln 100$	-
3	1.7	0.1	0.5	$\begin{pmatrix} 1.30 & 0.20 \\ -0.10 & 0.70 \end{pmatrix}$	$u_1 = \ln 50$	-
4	1.7	0.1	0.5	$\begin{pmatrix} 1.30 & 0.20 \\ -0.10 & 0.70 \end{pmatrix}$	$u_1 = \ln 1000$	-
5	1.7	0.1	0.5	$\begin{pmatrix} 1.10 & 0.40 \\ -0.10 & 0.90 \end{pmatrix}$	none	100, 10, -20, 15, 15
6	1.7	0.1	0.5	$\begin{pmatrix} 0.50 & -0.30 \\ -0.20 & 1.10 \end{pmatrix}$	none	100, 0, 20, 0, 20

Table 2: Multifractal and GSI parameters for the images in Colour Illustration 5.

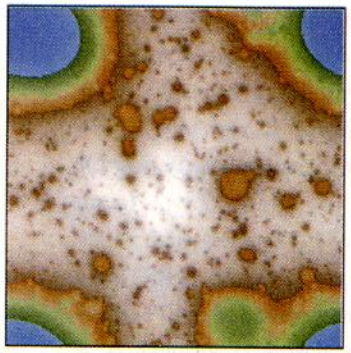

α=0.5 C_1=0.05

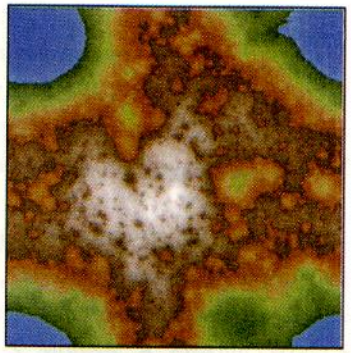

α=0.8 C_1=0.05

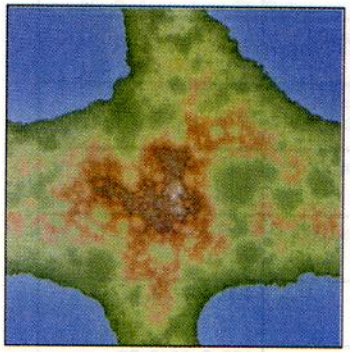

α=0.5 C_1=0.2

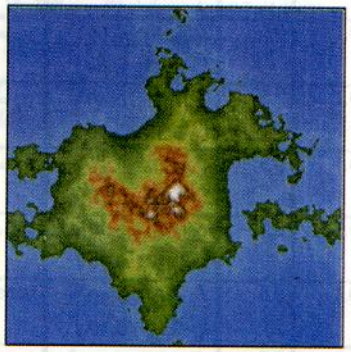

α=0.8 C_1=0.2

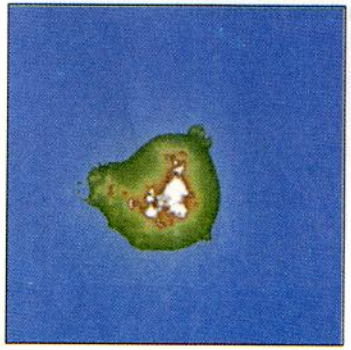

α=0.5 C_1=1.5

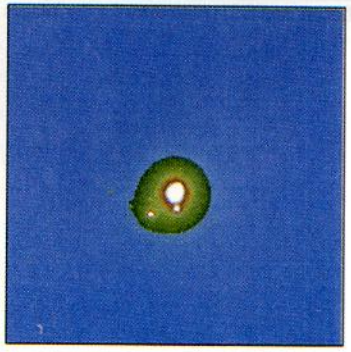

α=0.8 C_1=1.5

Colour Illustration 1.
2–D simulations , with varying α and C_1.
Seed is constant.
H–filtered with H=0.5
The palette is shown below. White values are high, blue low.

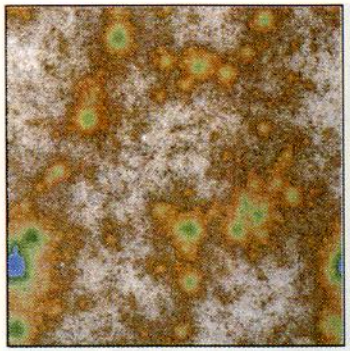

α=1.1 C_1=0.05

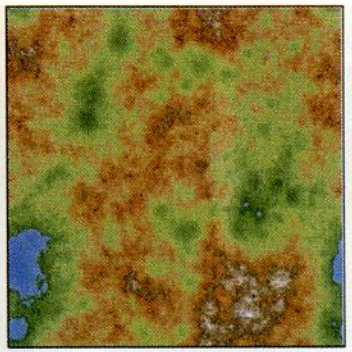

α=1.4 C_1=0.05

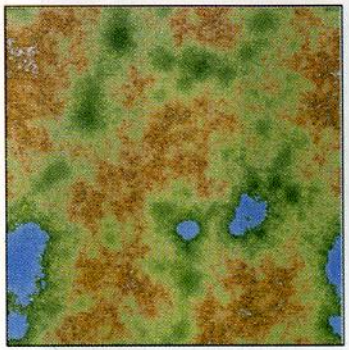

α=1.1 C_1=0.2

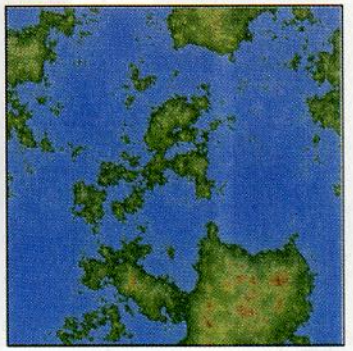

α=1.4 C_1=0.2

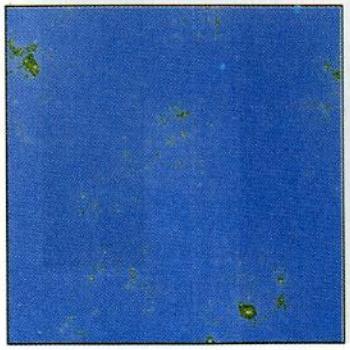

α=1.1 C_1=1.5

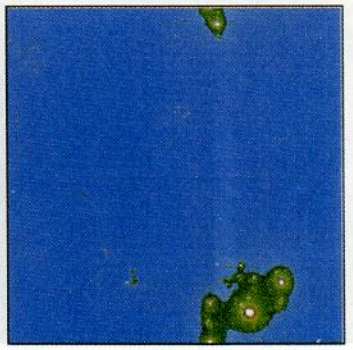

α=1.4 C_1=1.5

Colour Illustration 2.
2–D simulations , with varying α and C_1. Seed is constant. H–filtered with H=0.5
The palette is shown below. White values are high, blue low.

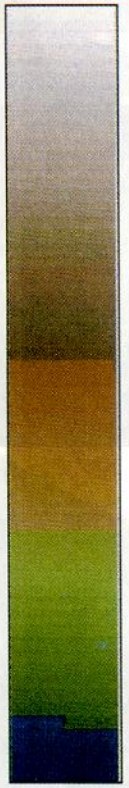

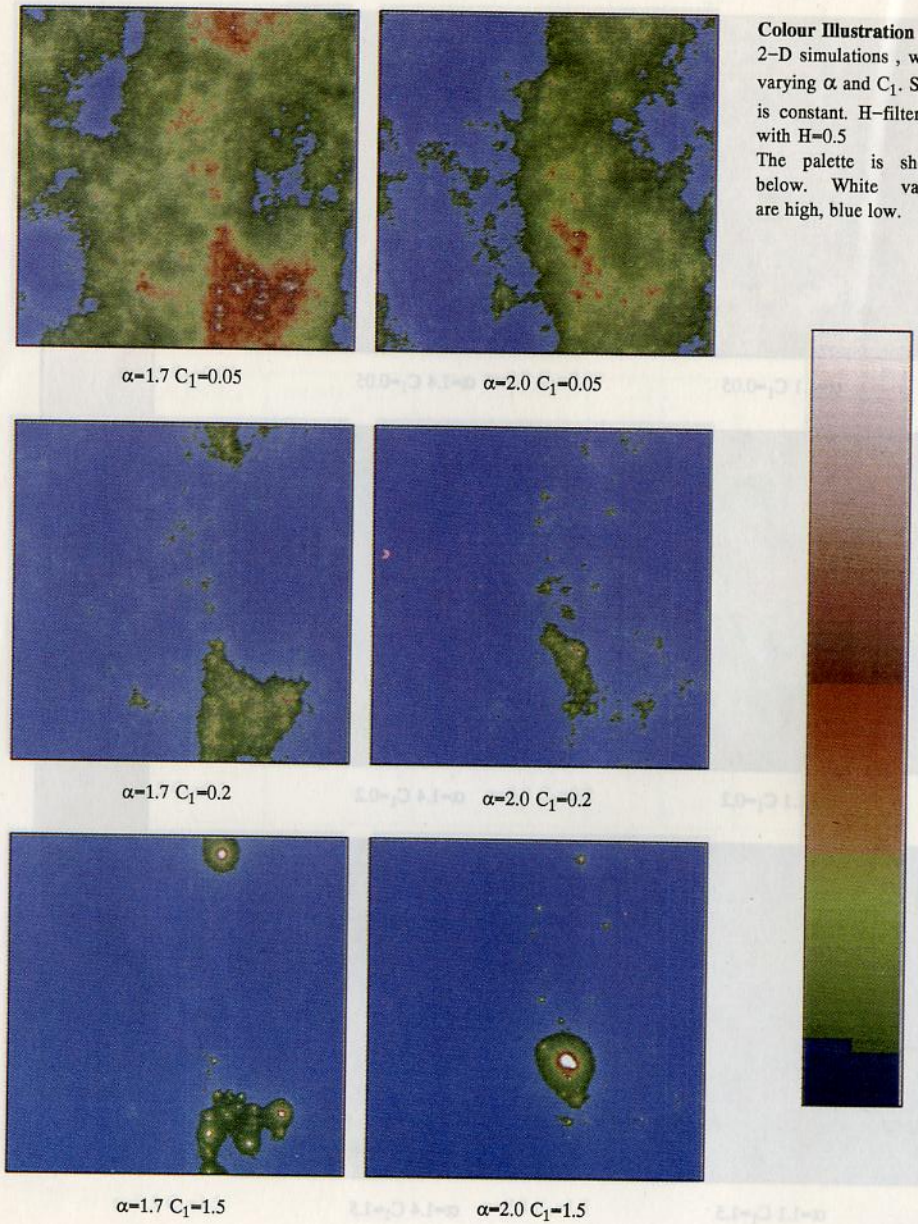

Colour Illustration 3. 2–D simulations , with varying α and C_1. Seed is constant. H–filtered with H=0.5
The palette is shown below. White values are high, blue low.

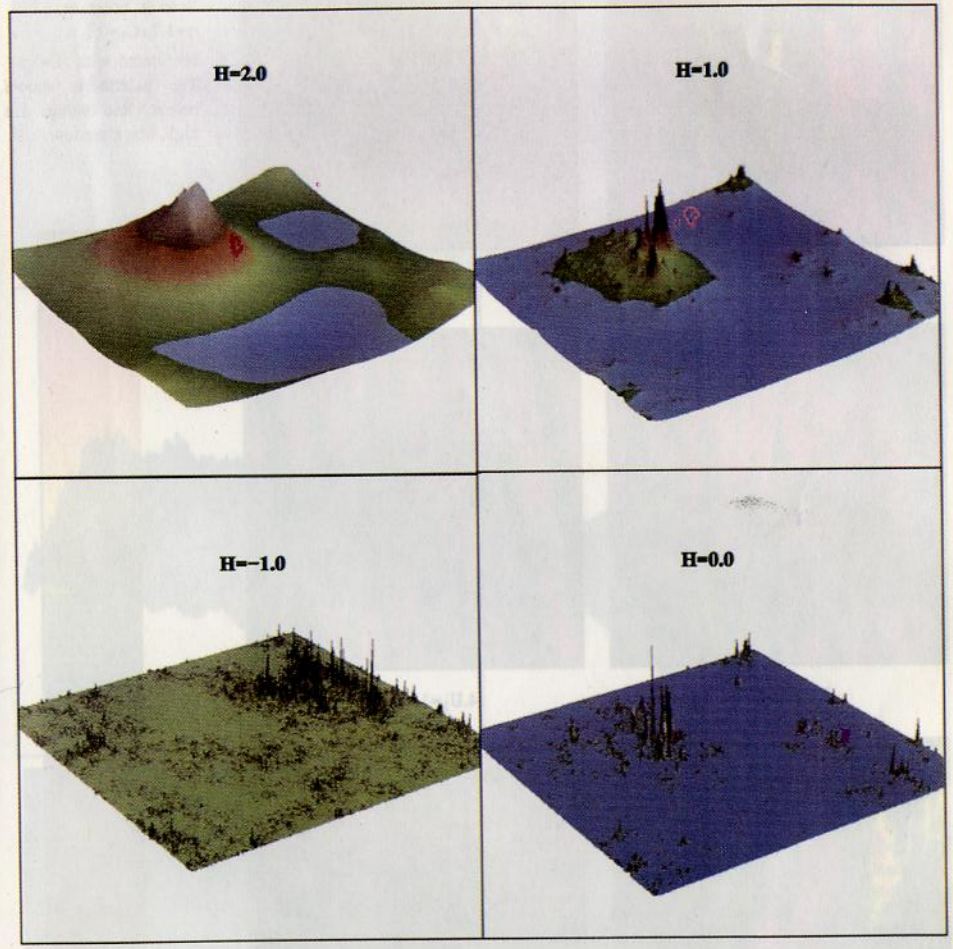

Colour Illustration 4. 3–dimensional representations of fields with α=1.7 and C_1=0.2, and variable H–filtering.

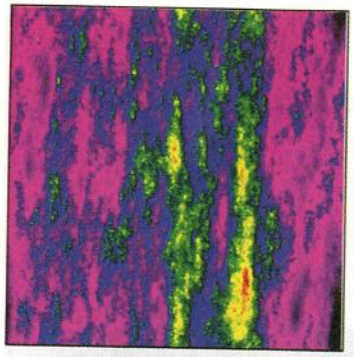

1.Stratification dominant

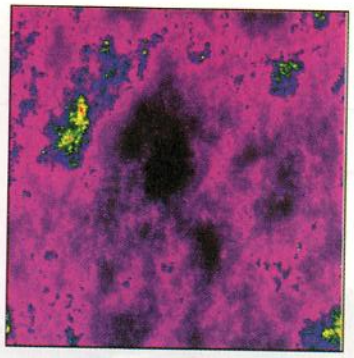

2.Rotation dominant

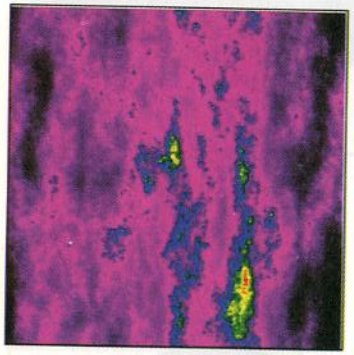

3.U_1=ln 50.0

4.U_1=1n1000.0

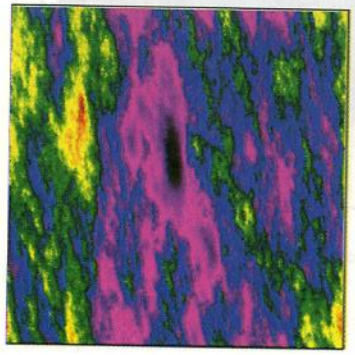

5.Non−spheroscale

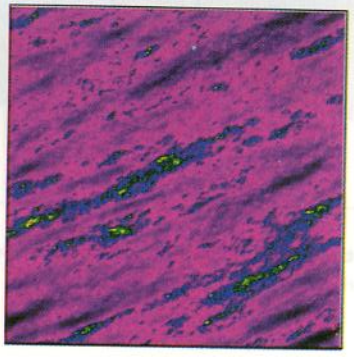

6.Non−spheroscale

Colour Illustration 5. 2−D simulations , with varying GSI parameters Seed is constant. α=1.7, C_1=0.1.

H−filtered with H=0.5 The palette is shown below. Red values are high, black are low.

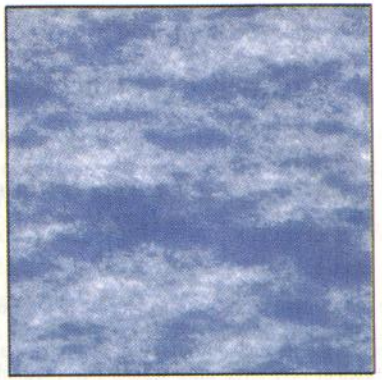

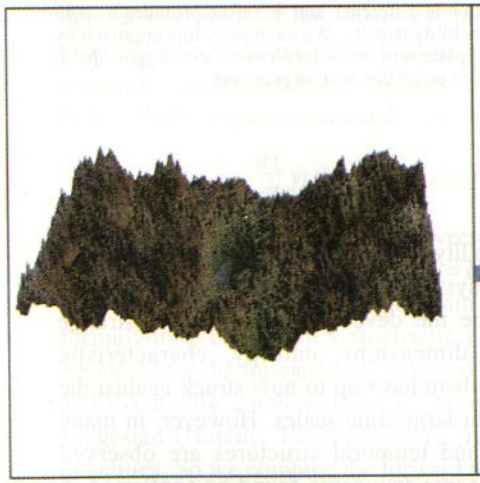

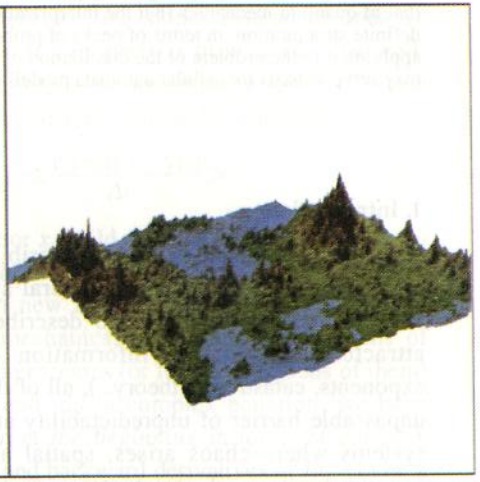

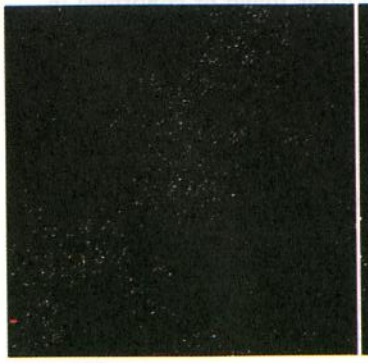

Colour Illustration 6. Simulations using parameters from Table 1. GSI was included. From top, two cloud simulations (visible spectrum),two topography simulations and two simulations of galactic luminosity distribution.